WEP Warwick Evans Publishing

International Journal of Mechanical and Electrical Engineering

ISSN: 3005-9615 (Print), ISSN: 3005-7132 (Online) | Volume 8, Number 1, Year 2026
DOI: https://doi.org/10.62051/ijmee.v8n1.03
Journal homepage: https://wepub.org/index.php/IJMEE/index

Research on Nondestructive Detection of Hawthorn Quality Based on Hyperspectral Imaging Technology

Jianwen Jiang, Shu Jiang

College of Electrical and Automation Engineering, East China Jiaotong University, Nanchang, Jiangxi, China

ABSTRACT

Hawthorn, a unique medicinal and edible economic crop in China, is prone to damage and pest infestations during harvesting and transportation, which severely degrade its quality and utilization value. Traditional manual and instrumental detection methods are characterized by low efficiency, strong subjectivity, and destructiveness, failing to meet the demands of large-scale quality inspection. This study focuses on hawthorn as the research object and conducts non-destructive detection of its damage and pests using hyperspectral imaging technology. By reviewing the domestic and foreign research progress in non-destructive detection of fruit damage, the application potential of hyperspectral imaging technology in the micro-damage and microcosmic detection of agricultural products is clarified. A technical route of "sample preparation—hyperspectral image acquisition—spectral preprocessing—model construction and validation" is designed. Spectral preprocessing is implemented via methods such as Standard Normal Variate (SNV) and Savitzky-Golay (SG) smoothing, and a detection system is established by integrating models including Partial Least Squares (PLS), Principal Component Regression (PCR), and Least Squares Support Vector Machine (LS-SVM). This study aims to address issues such as high sample misjudgment rate and redundant spectral information in hawthorn damage, with the expectation of achieving rapid, non-destructive, and accurate recognition. The research findings can provide technical support for quality grading and non-destructive detection in the hawthorn industry, as well as theoretical and practical references for the application expansion of non-destructive detection technology in agricultural products.

KEYWORDS

Hawthorn; Hyperspectral Imaging Technology; Non-destructive Detection; Damage Identification; Pest Detection; Model Construction.

1. INTRODUCTION

Traditional methods for hawthorn quality inspection primarily rely on manual labor and instruments, such as visual judgment to detect external damage, defects, and pest infestations. While these methods are highly accurate and the measurement techniques are relatively mature, they are time-consuming, labor-intensive, and destructive. Particularly for the intrinsic quality of the fruit, it is challenging to achieve large-scale inspection and quality grading. Specific limitations include: the measurement of intrinsic quality often requires sample pretreatment, which not only increases inspection time but also damages the samples, limiting their subsequent use or sale. When using manual assessment for external quality, a certain degree of subjectivity may arise, leading to issues such as inconsistent standards and unclear classification.

Significant research has been done on the early detection of hawthorn decay using non-destructive sensing technologies such as targeted the early damage of apples, collected spectral data in the range

of 400~1000 nm via hyperspectral imaging technology, and effectively distinguished apples with damage over 1 h from normal ones by selecting characteristic wavelengths and conducting stepwise discriminant analysis (Ding et al., 2021). Three apple varieties were taken as research objects for surface defect detection, with recognition accuracies of 76%, 85% and 95% respectively (Dan et al., 2020). Computer vision technology combined with deep learning algorithms was used to detect external defects of tomatoes; 43,843 tomato images were acquired, and external defects were detected through feature extraction and fine-tuning methods. The results showed that fine-tuning outperformed feature extraction, and ResNet50 was the optimal classification model, achieving an average accuracy of 94.6% on the test set (Costa et al., 2020). Using raw spectra and partial least squares discriminant analysis, a maturity recognition model with an accuracy of 91.53% was established, which effectively distinguished six maturity levels of Qingxiangjiao bananas (Chu et al., 2022).

For the acquired spectral data, the dual-wavelength combination method was adopted to identify effective wavelengths, and a partial least squares model was built to detect the color and firmness of Qingxiangjiao bananas, achieving favorable detection results (Xie et al., 2018). A non-destructive classification system for distinguishing banana quality and size was developed by combining RGB images, hyperspectral images and deep learning technology, which realized the classification of high-quality, ordinary and defective bananas with a classification accuracy of up to 98.45% (MESA et al., 2021). To detect Mycosphaerella fijiensis in the early stages of bananas, hyperspectral imaging technology was used to develop a partial least squares regression model with a prediction accuracy of 98% (UGARTE et al., 2020). Hyperspectral images of loquats with different damage degrees were collected; texture features of band ratio images were extracted via the Gray-Level Co-occurrence Matrix (GLCM), and combined with spectral data at three characteristic wavelengths in the near-infrared region to build a classification model, which achieved a classification accuracy of 91.3% (Li et al., 2022).

Hyperspectral images of persimmons at 0, 1, 2 and 3 days after damage were collected, and spectral data were analyzed based on the Principal Component Analysis (PCA) algorithm; 90.0% of healthy fruits and 90.8% of damaged fruits were correctly classified. A Partial Least Squares Discriminant Analysis (PLS-DA) model was established, calibrated using the average spectra of detected damaged pixels, with an overall accuracy of 99.4% (Munera et al., 2021). Raghavendr et al. established a classification model for defective and healthy mangoes using a near-infrared spectral dataset in the wavelength range of 673~1900 nm. The Fisher discriminant method was used to find the optimal wavelengths for mango defect detection in the range of 702.72-752.34 nm, with a classification accuracy of 84.5% (Raghavendr et al., 2021). Hyperspectral imaging in the range of 450-1040 nm was applied to detect mechanical damage of persimmons without any external symptoms, with a correct rate of 90.8% (Munera et al., 2019).

Visible/near-infrared reflectance was used to detect the sunburn degree of apples. A portable instrument was employed to collect apple spectral data, and the IPLS-DA model was used for multivariate analysis (Grandón et al., 2018). The data were processed by Principal Component Analysis (PCA), and after selecting Regions of Interest (ROI) according to certain rules, multiple extraction models were established and compared. The results showed that the Random Forest (RF) model had high and stable classification accuracy, with an average accuracy of 99.9% (Che et al., 2011).

Vis/NIR hyperspectral imaging combined with image-spectral fusion processing technology was used to detect early decay of tomatoes, and an LS-SVM recognition model was established. The study found that the model built by fusing the G component of RGB images with the corrected single-wavelength image information at 666 nm achieved a recognition rate of 100% for decayed fruits and 97.5% for intact fruits (Wang et al., 2020).

2. MATERIALS AND METHODS

2.1. Fruit Samples

In this study, 200 samples of 'Dajinxing' hawthorn were selected as experimental subjects. Firstly, the core internal quality indicators of the samples, including total acid content, vitamin C content, and soluble solid content, were accurately determined using national standard physicochemical detection methods. Meanwhile, hyperspectral data of the samples were collected by a hyperspectral imaging system to obtain continuous spectral curves that characterize the internal material properties of hawthorn fruits. The hyperspectral data of hawthorn were correlated and matched with the measured physicochemical data of internal quality, which were then used as model input parameters. Combined with chemometric algorithms, a quantitative analysis model for the internal quality of hawthorn was constructed, and ultimately a comprehensive detection model for hawthorn quality integrating multiple indicators (total acid, vitamin C, and soluble solids) was established.

2.2. Sample Data Acquisition

The samples were placed on the sample stage inside the dark box illustrated in Fig.1, after which the hyperspectral images depicted in Fig.2 were acquired. For each sample, spectral scanning was performed consecutively three times, and the average spectrum derived from the three spectral profiles was adopted as the final raw spectrum.

Fig 1. Samples in the camera obscura

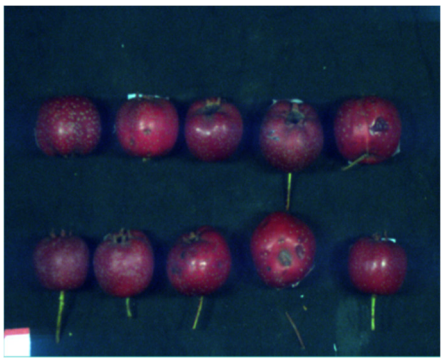

Fig 2. Hyperspectral image of the sample

To eliminate the effects of system noise, light source inhomogeneity, and dark current on imaging quality, black-white calibration was performed prior to sample acquisition. White calibration involved placing a standard diffuse reflection whiteboard at the center of the stage and capturing its hyperspectral image, which served as the reference for full-spectrum reflectance. For black calibration, the light source was turned off and the camera lens cap was covered to capture an image under complete darkness, which was used as the reference for dark current. The right figure shows the black and white boards used in the experiment, and the calculation formula for black-white calibration is as follows:

$$R_c = \frac{I_c - I_d}{I_w - I_d} \tag{1}$$

In Equation (1), R_c denotes the calibrated image, I_c represents the initial raw image, I_d stands for the dark calibration image, and I_w refers to the whiteboard image used for calibration.

2.3. Average Spectra of Hawthorn Samples

Fig.3 displays the average reflectance spectral curves of hawthorn samples in the near-infrared (NIR) wavelength range of 900–1800 nm, which reflect the absorption and reflection characteristics of hawthorn pulp, peel, and internal chemical components (e.g., moisture, sugar, organic acids) to NIR

light of different wavelengths. The overall curve shows a trend of slight fluctuating increase followed by a continuous decrease, reaching a trough at around 1500 nm, and finally a slow recovery, which is highly consistent with the NIR absorption characteristics of the main components in hawthorn.

(1) 900–1100 nm: Slight fluctuation stage

The reflectance fluctuates within the range of 0.6–0.7, with a minor trough at 1000 nm and a peak at 1100 nm. This wavelength band corresponds to the weak absorption band of moisture in hawthorn (the sideband of the first overtone absorption of water in the NIR region), and is simultaneously affected by the light scattering of peel pigments (e.g., anthocyanins, carotenoids).

(2) 1100–1500 nm: Rapid decline stage

The reflectance decreases continuously from approximately 0.7 to around 0.15 at 1500 nm, representing the most significant decline interval of the curve. The 1200–1400 nm range is the strong absorption band of moisture (the first overtone absorption of O-H bonds in water, centered at about 1450 nm). With the pulp moisture content of hawthorn ranging from 70% to 80%, the intense absorption of light in this band by a large amount of moisture constitutes the core reason for the sharp decline in reflectance. Meanwhile, it is superimposed with the C-H bond vibrational absorption of sugars (fructose, glucose) centered at about 1350 nm, which further reduces the reflectance. In addition, the weak absorption of short-wavelength NIR light by pigments leads to slight fluctuations in reflectance.

(3) 1500–1800 nm: Recovery stage

The reflectance gradually recovers from the trough at 1500 nm to approximately 0.3 at 1700 nm, followed by a slight decrease.

Mechanism: The absorption intensity of moisture weakens in this band, and the reflectance is mainly dominated by the combination band absorption of C-H and O-H bonds in carbohydrates (pectin, cellulose) in hawthorn and the light scattering characteristics of pulp tissue. The weak light absorption by macromolecular carbohydrates results in a gradual recovery of reflectance. The slight decline after 1700 nm is associated with the C=O bond absorption of organic acids (e.g., citric acid).

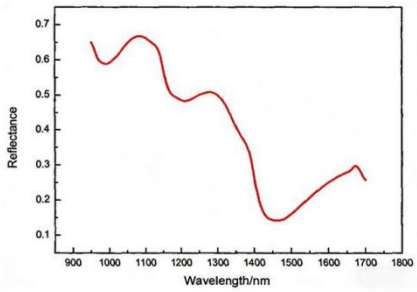

Fig 3. The average spectrum of hawthorn samples

The spectral range of 1400–1500 nm corresponds to the characteristic absorption peak of moisture, which can serve as the core band for the non-destructive detection of water content in hawthorn. Variations in reflectance within the ranges of 1300–1400 nm (for sugars) and 1600–1700 nm (for organic acids) are applicable for constructing prediction models for soluble solid content and total acid content in hawthorn. The fluctuation characteristics in the 900–1100 nm range can be used as an auxiliary indicator to distinguish the peel quality of hawthorn, while the recovery trend after 1500 nm is capable of reflecting differences in the fiber content of hawthorn pulp.

2.4. Spectral Data Preprocessing

In this study, the near-infrared spectra of hawthorn were taken as the research object, and the raw spectra were subjected to noise reduction processing via different preprocessing methods, including

Multiplicative Scatter Correction (MSC), Standard Normal Variate transformation (SNV), Savitzky-Golay (SG) smoothing, first derivative and second derivative, respectively.

The preprocessing methods with relatively high accuracy were further compared. The results indicated that the second-order three-point SG smoothing achieved the highest coefficient of determination of the calibration set (Rc^2), the lowest root mean square error of the calibration set (RMSEC), and the minimal gap between Rc^2 and coefficient of determination of the prediction set (Rp^2), demonstrating superior system prediction performance. A comprehensive comparison revealed that second-order three-point SG smoothing was the optimal choice for single-factor preprocessing of hawthorn hyperspectral data. In contrast, the combined preprocessing method of SNV + SG (3,2) achieved the comprehensive optimization of the performance of Partial Least Squares (PLS) prediction models for various quality indicators, thereby providing reliable preprocessing technical support for subsequent non-destructive detection of hawthorn quality.

Table 1. Results of PLS Prediction Models with Different Preprocessing Methods

Preprocessing Methods	Calibration Set for Soluble Solids		Calibration Set for Acids		Calibration Set for Vitamin C		Calibration Set for Hardness	
	Rc^2	RMSEC	Rc^2	RMSEC	Rc^2	RMSEC	Rc^2	RMSEC
RAW	0.3719	0.4915	0.3249	0.3589	0.6341	1.6846	0.7789	24.8424
SG(3,1)	0.6376	0.3733	0.5783	0.2836	0.7038	1.5157	0.8598	19.7854
SG(3,2)	0.9270	0.1675	0.8922	0.0143	0.9215	0.7801	0.9026	16.4853
SG(9,2)	0.4782	0.4480	0.4219	0.0332	0.6425	1.6652	0.8344	21.5009
SNV	0.3304	0.5075	0.3197	0.0360	0.5929	1.7768	0.7900	24.2095
MSC	0.3291	0.5080	0.3266	0.0359	0.5926	1.7775	0.7902	24.2095
SNV+SG(3,2)	0.8535	0.2374	0.8703	0.1557	0.8799	0.9649	0.8873	17.7374
MSC+SG(3.2)	0.8524	0.2382	0.8574	0.0165	0.8754	0.9830	0.8863	17.8195

3. MODELING AND ANALYSIS

3.1. Modeling Based on Full-Spectrum PLS

During the modeling process, the full-waveband hyperspectral data of the calibration set samples were employed as independent variables, while the laboratory-measured internal quality indicators (including soluble solids, acids, vitamin C, and firmness) were designated as dependent variables to construct a Partial Least Squares (PLS) regression prediction model. The calibration fitting effect and prediction performance of the model were presented via the quantitative indicators listed in Table 2.

Table 2. Prediction Results of Full-Spectrum PLS Modeling

PC	Calibration Set for Soluble Solids		Calibration Set for Acids		Calibration Set for Vitamin C		Calibration Set for Hardness	
	Rc^2	RMSEC	Rc^2	RMSEC	Rc^2	RMSEC	Rc^2	RMSEC
10	0.3719	0.4915	0.3249	0.3589	0.6341	1.6846	0.7789	24.8424

As can be seen from the prediction results of the Partial Least Squares (PLS) models for the four hawthorn quality indicators presented in the fig.4, the coefficients of determination (R^2) corresponding to each indicator are 0.8460, 0.6992, 0.8331 and 0.8384, respectively. Comparative analysis reveals that except for the acidity indicator, whose R^2 is only 0.6992 and fails to reach a high prediction accuracy, the R^2 values of the other three quality indicators fall within the range of

0.83–0.85. The prediction results achieve high accuracy and can well reflect the correlation between hyperspectral data and the internal quality of hawthorn.

Combined with the analysis of the experimental procedure, there was a relatively long time interval between the acquisition of hyperspectral image data and the determination of internal quality indicators of hawthorn in this study. During this period, physiological and metabolic changes may have occurred in hawthorn pulp, which led to a weakened correlation between the measured values of the acidity indicator and the spectral data. This is probably the main reason for the unsatisfactory prediction results of the acidity indicator.

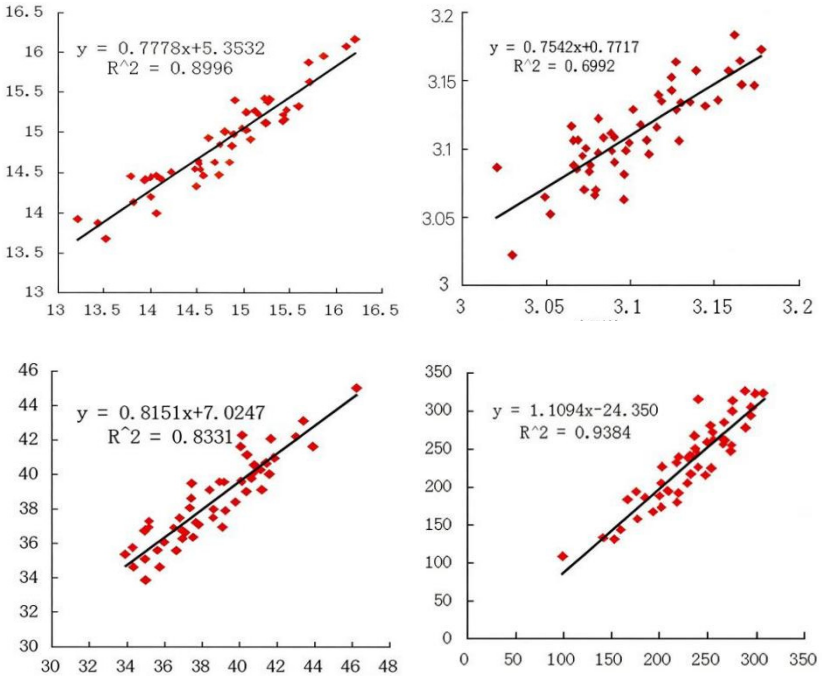

Fig 4. The prediction results of the PLS model

3.2. Modeling Based on Full-Spectrum PLS -SVM

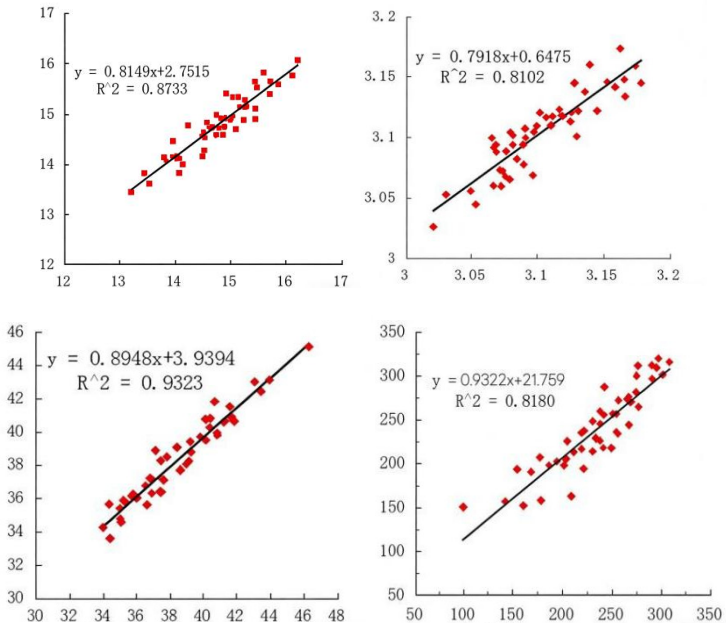

Fig 5. The LS-SVM model prediction results

As can be seen from the prediction results of the Least Squares Support Vector Machine (LS-SVM) models for the four quality indicators presented in the fig.5, the coefficients of determination (R^2) calculated by the corresponding indicator models are 0.8733, 0.8102, 0.9323 and 0.8180, respectively. Among these values, the R^2 of the vitamin C indicator reaches 0.9323, indicating that the model has a high level of fitting degree and prediction accuracy for this indicator. The R^2 values of the other three indicators are all distributed in the range of 0.81–0.88, which also reflects good prediction performance. Overall, the LS-SVM models for the four indicators can well establish the correlation between hyperspectral data and hawthorn quality indicators, and the overall prediction results achieve high accuracy, which can meet the practical application requirements for the non-destructive detection of hawthorn quality.

3.3. Modeling and Analysis of Characteristic Wavebands

In this study, the Successive Projections Algorithm (SPA) was employed to screen the sensitive characteristic wavelengths for hawthorn quality indicators. The calculation was performed with 1 set as the minimum effective wavelength number and 10 as the maximum wavelength number.

As indicated by the error curve analysis, the root mean square error (RMSE) of the four quality indicators reached the global minimum when the number of selected characteristic wavelengths was 7 (for soluble solids), 7 (for acidity), 7 (for vitamin C), and 6 (for firmness), with the corresponding values being 0.4843 Brix, 0.0343 (acidity unit), 1.6481 mg/100g, and 33.2332 (firmness unit), respectively.

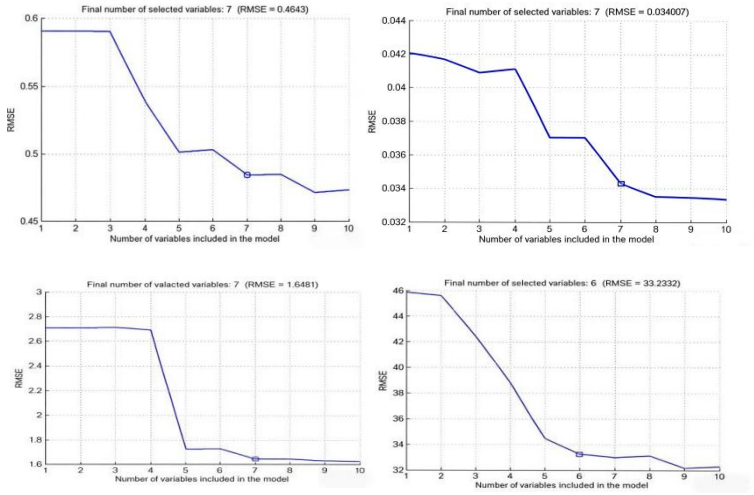

Fig 6. Error graph of the successive projections algorithm

Based on the aforementioned optimal screening results, this study selected the four groups of characteristic wavebands shown in the figure for fusion processing, and finally obtained 22 non-redundant optimal characteristic wavelengths.

These characteristic wavelengths were denoted as a001, a011, a013, a014, a018, a060, a065, a068, a081, a085, a115, a117, a127, a131, a152, a161, a163, a184, a228, a243, a244 and a254 in sequence.

Their corresponding actual wavelength values were 895.9 nm, 927.83 nm, 934.21 nm, 937.41 nm, 950.16 nm, 1084.11 nm, 1100.06 nm, 1109.61 nm, 1151.04 nm, 1163.79 nm, 1259.31 nm, 1266.60 nm, 1297.51 nm, 1310.22 nm, 1377.03 nm, 1405.65 nm, 1412.01 nm, 1478.75 nm, 1618.47 nm, 1666.07 nm, 1669.25 nm and 1700.96 nm, respectively.

3.4. Modeling Based on PLS of Characteristic Wavebands

Taking the hyperspectral data of the characteristic wavebands of the calibration set samples as the independent variables, and the internal quality indicator data obtained from laboratory

physicochemical detection as the dependent variables, a partial least squares (PLS) quantitative prediction model was constructed. The evaluation results of the model's fitting accuracy and prediction performance are presented in Table 3 and Figure 8. The analysis results demonstrate that the PLS model established solely based on the characteristic waveband spectral data exhibits low goodness-of-fit for the calibration set and large prediction deviations for the quality indicators of the prediction set samples, meaning that the overall modeling and prediction performance fails to meet the expected requirements.

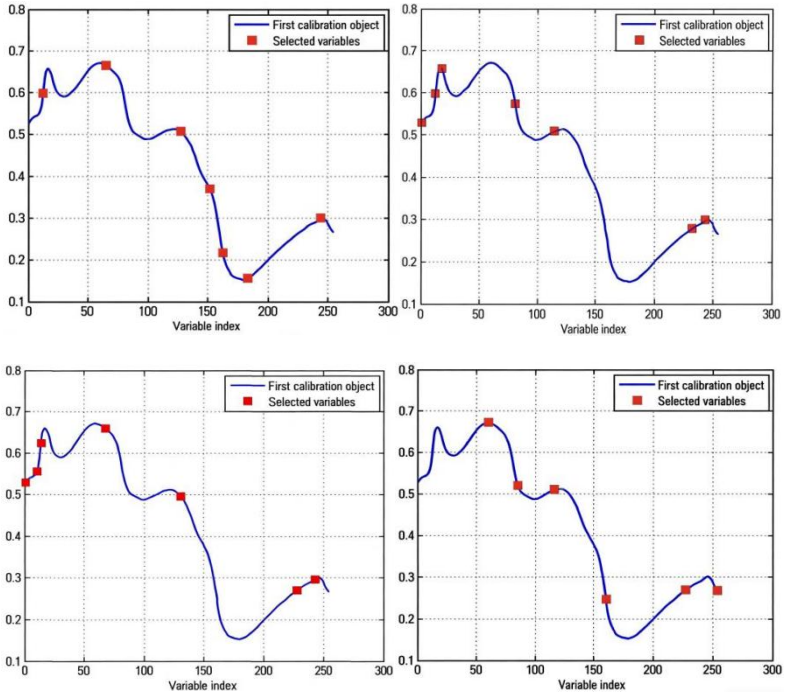

Fig 7. Characteristic wavelengths extracted by the successive projections algorithm

Table 3. Prediction Results of PLS Modeling Based on Characteristic Wavebands

PC	Calibration Set for Soluble Solids		Calibration Set for Acids		Calibration Set for Vitamin C		Calibration Set for Hardness	
	Rc^2	RMSEC	Rc^2	RMSEC	Rc^2	RMSEC	Rc^2	RMSEC
Optimal Parameters	0.3025 4	0.4883 6	0.5504 2	0.0297 5	0.4391 7	2.0633 6	0.6248 5	31.9134 9

The R^2 values of the four groups of models all failed to reach the high fitting level of over 0.8, indicating that the current PLS models still have room for optimization in predicting hawthorn quality indicators. Among them, the model corresponding to the first figure exhibited the best performance, while that corresponding to the second figure performed the worst. The abnormal points in the low measured value region might be caused by inherent sample differences or insufficient preprocessing of hyperspectral data. It is necessary to further optimize the modeling methods (e.g., characteristic wavelength screening, data denoising, and introduction of nonlinear models) to improve the prediction accuracy.

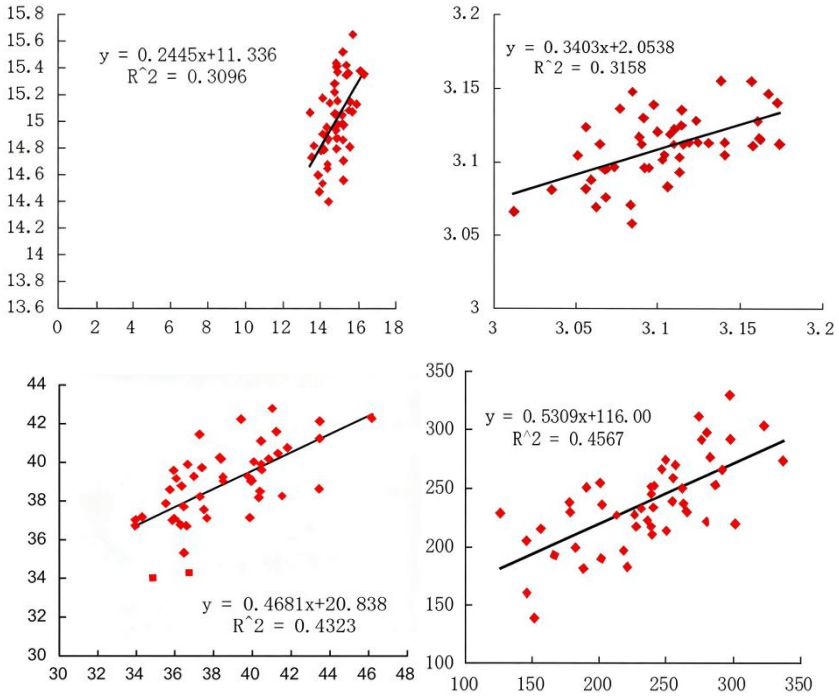

Fig 8. Prediction results of PLS model based on characteristic wavelengths

3.5. Modeling Based on PLS-SVM of Characteristic Wavebands

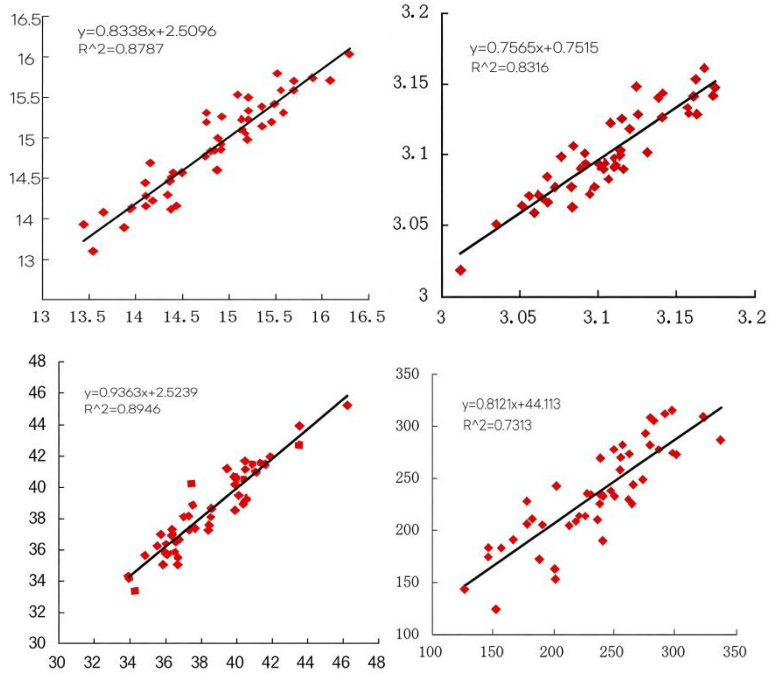

Fig 9. Prediction results of LS-SVM model based on characteristic wavelengths

The coefficients of determination (R^2) for the prediction of each quality indicator ranged from 0.7313 to 0.8946, with significant differences in prediction accuracy observed among the indicators. Specifically, the R^2 value of the third indicator reached 0.8946, representing the optimal prediction performance; the R^2 values of the first and second indicators were 0.8787 and 0.8316, respectively, indicating good prediction reliability.

In contrast, the R^2 value of the fourth indicator was only 0.7313, and its fitting accuracy was relatively low due to the scattering of data points away from the fitting line and the presence of outliers. The fitting slopes of all indicators were close to 1, which demonstrated that the predicted values exhibited a reasonable linear growth trend with the measured values, thus verifying the effectiveness of characteristic wavelength screening and the applicability of the LS-SVM model. For the fourth indicator with low prediction accuracy, the robustness of the model could be improved in subsequent studies by optimizing the characteristic wavelength screening algorithm and introducing an outlier elimination strategy.

As for the first three indicators with high prediction accuracy, the generalization ability of the model could be further enhanced by expanding the sample size and integrating multi-source feature fusion methods, which would provide more accurate technical support for the high-throughput non-destructive detection of hawthorn quality.

4. CONCLUSION

In the research on non-destructive detection of hawthorn quality, to achieve accurate quantitative analysis of four core quality indicators including soluble solids, acidity, vitamin C, and firmness, this study constructed four comprehensive multi-quality prediction models, namely Partial Least Squares (PLS), Least Squares Support Vector Machine (LS-SVM), Successive Projections Algorithm combined with Partial Least Squares (SPA-PLS), and Successive Projections Algorithm combined with Least Squares Support Vector Machine (SPA-LS-SVM).

Taking the measured data of the four quality indicators as the reference, this study conducted a systematic comparative analysis of the performance parameters and prediction results of the above four models based on the prediction set samples. The results showed that the SPA-LS-SVM model established with the 22 characteristic wavelengths screened by the Successive Projections Algorithm as input parameters exhibited the optimal performance in the prediction of all quality indicators. Its coefficients of determination for the prediction set (R^2_p) for soluble solids, acidity, vitamin C, and firmness reached 0.8787, 0.8316, 0.8946, and 0.7313, respectively, which provides a reliable technical solution for the rapid and efficient detection of hawthorn quality.

DATA AVAILABILITY STATEMENT

The original contributions presented in this study are included in the article, further inquiries can be directed to the corresponding author.

CONfIICT OF INTEREST

The authors declare that they have no known competing ffnancial interests or personal relationships that could have appeared to inffuence the work reported in this paper.

REFERENCES

[1] Ding C Q, FENG Z, WANG D C, CUI D, LI W H. Acoustic vibration technology: Toward a promising fruit quality detection method [J]. Comprehensive Reviews in Food Science and Food Safety, 2021,20:1655-1680. DOI: 10.1111/1541-4337.12722.

[2] Dan S. NIR spectroscopy fruit quality detection algorithm based on the least angle regression model [J]. International Journal of High Performance Systems Architecture, 2020,9(2/3):128-135. DOI:10.1504/IJHPSA. 2020. 10033757.

[3] Costa A Z, Figueroa H E H, Fracarolli J A. Computer vision based detection of external defects on tomatoes using deep learning [J]. Biosystems Engineering, 2020, 190: 131-144.

[4] Chu X, MIAO P, ZHANG K, et al. Green banana maturity classification and quality evaluation using hyperspectral imaging [J]. Agriculture, 2022, 12(4): 53-61.

[5] Xie C, CHU B, HE Y. Prediction of banana color and firmness using a novel wavelengths selection method of hyperspectral imaging [J]. Food Chemistry, 2018, 245: 132-140.

[6] MESA, ARMACHESKA R, CHIANG J. Multi-input deep learning model with rgb and hyperspectral imaging for banana grading [J]. Agriculture, 2021, 11(8): 68-87.

[7] UGARTE F J, BAYONA A O, CRIOLLO B R, et al. Early detection of black Sigatoka in banana leaves using hyperspectral images [J]. Applications in Plant Sciences, 2020, 8(8): 113-129.

[8] Li B, Han Z, Wang Q, et al. Study on qualitative impact damage of loquats using hyperspectral technology coupled with texture features [J]. Foods, 2022, 11(16): 2444. [26] Munera S, Rodríguez-Ortega A, Aleixos N, et al. Detection of invisible damages in 'Rojo

[9] Raghavendra A, Guru D S, Rao M K. Mango internal defect detection based on optimal wavelength selection method using NIR spectroscopy [J]. Artificial Intelligence in Agriculture, 2021, 5: 43-51.

[10] Munera S, Rodríguez-Ortega A, Aleixos N, et al. Detection of invisible damages 'inrojo brillante' persimmon fruit at different stages using hyperspectral imaging and chemometrics [J]. Foods, 2021, 10(9): 2170.

[11] Grandón S, Sanchez-Contreras J, Torres C A. Prediction models for sunscald onapples using Vis-NIR reflectance [J]. Postharvest Biology and Technology, 2019, 151: 36-44.

[12] Che W, Sun L, Zhang Q, et al. Pixel based bruise region extraction of apple using Vis-NIR hyperspectral imaging[J]. Computers and Electronics in Agriculture, 2018, 146: 12-21.

[13] Mendoza F, Lu R F, Ariana D, et al. Integrated spectral and image analysis of hyperspectral scattering data for prediction of apple fruit firmness and soluble solids content [J]. Postharvest Biology and Technology, 2011, 62(2): 149-60.

[14] Wang C, Wang S, He X, et al. Combination of spectra and texture data of hyperspectral imaging for prediction and visualization of palmitic acid and oleic acid contents in lamb meat [J]. Meat Science, 2020, 169: 108194.